Shear failure of RC elements strengthened with steel profiles and CFRP wraps

Massimiliano Bocciarelli [a], Serena Gambarelli [b], Nicola Nisticò [b], Marco Andrea Pisani [a,*], Carlo Poggi [a]

[a] Department of Architecture, Built Environment and Construction Engineering, Politecnico di Milano, Piazza Leonardo da Vinci 32, 20133 Milano, Italy
[b] Department of Structural and Geotechnical Engineering, University of Rome La Sapienza, via Eudossiana 18, 00184 Roma, Italy

Received 9 April 2014
Received in revised form 22 May 2014 Accepted 16 June 2014
Available online 22 June 2014

1. Introduction

Composite materials like CFRP (Carbon Fiber Reinforced Polymer) have become very popular for the retrofitting of existing structural members. The reason for this popularity is well known: the technology combines the mechanical properties of this composite material with the advantages related to the installation process simplified by their easy handling.

Many studies [1–7] have been devoted to this strengthening technique, outlining two different failure modes for the retrofitted beams: tensile rupture of the FRP or debonding of the FRP from the sides of the RC element. The failure mode in turn depends on the strengthening configuration, which is (see Fig. 1): full wraps (FW), U-jackets (UJ), or side strips (SS). The fully wrapped configuration is the most efficient one, since FRP debonding from concrete, even if present, does not significantly reduce the ultimate FRP strength, differently from what happens with the U-jackets and side strips configuration, whose efficiency rely only on the debonding resistance. In the case of side strips crack-bridging mechanism is evident, whereas the Mörsch truss resisting mechanisms applies to full wraps [8–10].

Most of the proposed predictive expressions are tailored for classical configurations where the FRP is directly applied to the concrete surface and the FRP stress is strongly affected by the crack evolution, which induces into the reinforcement a significant transversal strain due to the relative displacement of the two faces of the crack.

This strong and negative interaction between FRP transversal strain and concrete crack evolution can be minimized (as here proposed) by creating a gap between FRP and concrete: four steel angles can be applied at the four section corners (glued to the concrete surface) and the FRP strips can be wrapped around the section being in contact with the steel angles but not with the concrete surface. The gap between the FRP and the concrete surface can be eventually filled with mortar.

The proposed technology has been already analyzed in [11] in order to evaluate its performance in terms of axial ductility and increase in axial load capacity; its validation for shear increase will be presented in the following, by describing the experimental tests carried out, whose outcomes will be compared with the design equations proposed in the ACI [12] code and Italian CNR guidelines [13].

2. Shear design of RC elements

The shear behavior of reinforced concrete beams and columns is often presented and explained by the truss mechanism derived from the model by Ritter and Mörsch [8–10]. According to this model a concrete strut angle (θ) equal to 45° is assumed and the element capacity is evaluated by means of the contribute (V_s) of the steel shear reinforcement. Other approaches have been proposed in the literature, recognizing the importance of considering other resistant contributes, such as those due to aggregate

* Corresponding author. Tel.: +39 0223994398; fax: +39 0223994220.
E-mail address: marcoandrea.pisani@polimi.it (M.A. Pisani).

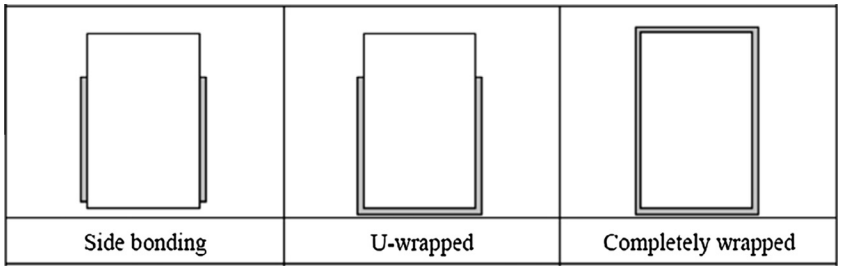

Fig. 1. Cross section of FRP strengthened elements.

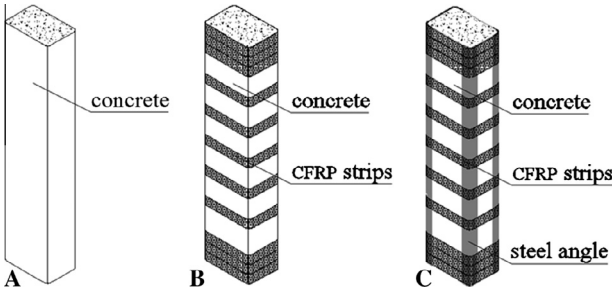

Fig. 2. CFRP shear resisting mechanism: (A) reference element; (B) CFRP strips and (C) CFRP strips and steel angles.

interlocking, dowel effect of the longitudinal bars and axial load. Additive expressions that combine V_s (steel contribute) and V_c (concrete contribute) have been presented, such as the predictive equation proposed in [14], where V_s is simply added to the concrete (V_c) and axial load (V_p) contributions. Other proposals [15] include all contributions, without explicitly considering the concrete one, allowing to assume a variable concrete truss angle (θ) lower than (or equal to) 45° and greater than ~22°.

Regarding FRP reinforced elements, traditional approaches adopt the model proposed for steel reinforced concrete, recognizing that a crucial aspect is the evaluation of the effective strain distribution in the FRP stirrups, especially across the crack, where, independently of the adopted configuration (FW, UJ, SS), stress concentrations are present due to the debonding process. The problem is solved assuming a reduced FRP strength or strain, either empirically evaluated, such as in the American code [12], or based on an analytical approach such as that proposed in [4] and included in the Italian guidelines [13].

When dealing with the Italian guidelines, the shear strength depends on the FRP reinforcement contribution ($V_{Rd,f}$) and on design shear resistance provided by stirrups of the original element, not yet retrofitted ($V_{Rd,s}$):

$$V_{Rd} = min\{V_{Rd,s} + V_{Rd,f}, V_{Rd,c}\} \tag{1a}$$

where $V_{Rd,c}$ is the design strength of the concrete compression strut.

The FRP shear resistance $V_{Rd,f}$ may be assessed by Eq. (1b),

$$V_{Rd,f} = \frac{1}{\gamma_{Rd}} \cdot 0.9d \cdot f_{fed} \cdot 2 \cdot t_f \cdot cot\theta \cdot \frac{b_f}{p_f} \tag{1b}$$

where:

- γ_{Rd} is a partial factor, set equal to 1.2;
- d is the member effective depth;
- θ the concrete truss angle;
- t_f, b_f and p_f are FRP thickness, width and spacing, respectively;
- f_{fed} is the effective FRP design strength that, taking into account the debonding process, is lower than the FRP design strength (f_{fd}):

The value of the effective FRP design strength (f_{fed}) is evaluated according to the following expression:

$$f_{fed} = f_{fdd} \cdot \left[1 - \frac{1}{6}\frac{l_e}{0.9 \cdot d}\right] + \frac{1}{2}\left[\left(0.2 + 1.6\frac{r_c}{b_w}\right) \cdot f_{fd} - f_{fdd}\right] \cdot \left[1 - \frac{l_e}{0.9 \cdot d}\right] \tag{2a}$$

Table 1
Geometry and shear strengthening configurations of the specimens.

ID	Layers Number	Wrapping spacing	Steel profiles	Bottom reinforcement	Thixotropic mortar	Shear reinforcement
REF	–	–	–	5 ϕ 20	–	
CW90/30	1	30	–	5 ϕ 20	–	
CW90-8.6/30	1	30	80 × 6	5 ϕ 20	6 mm	
CW90-8.6/30*	1	30	80 × 6	5 ϕ 20	–	
CW90-8.6/30D	2	30	80 × 6	5 ϕ 20	6 mm	
M + CW90-8.6/30D	2	30	80 × 6	7 ϕ 20	6 mm	
M + CW90-12.8/30D	2	30	120 × 8	7 ϕ 20	8 mm	
CW90-8.6/30D*	2	30	80 × 6	5 ϕ 20	–	
CW90-8.6/60	2	60	80 × 6	5 ϕ 20	6 mm	

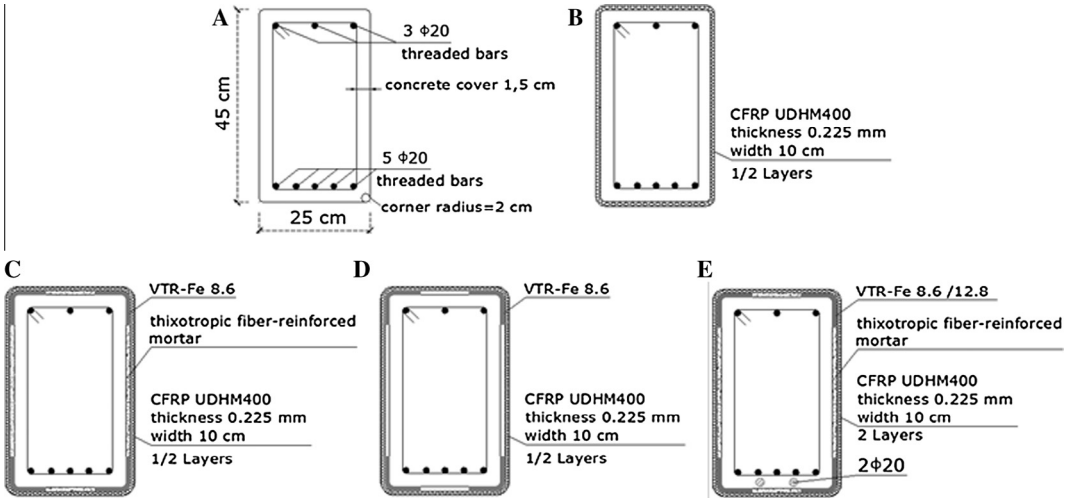

Fig. 3. main cross sections of the tested elements: (A) REF; (B) CW90/30; (C) CW90-8.6/30, CW90-8.6/30D, CW90-8.6/60; (D) CW90-8.6/30*, CW90-8.6/30D*; (E) M + CW90-8.6/30D, M + CW90-12.8/30D.

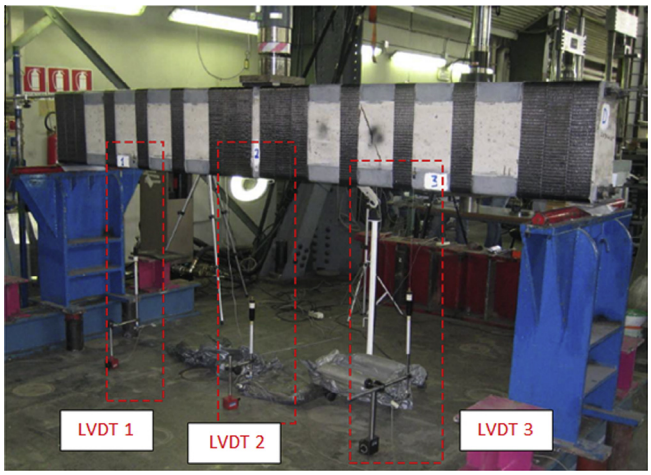

Fig. 4A. Test set-up with free core displacement transducers (LVDT 1,2,3).

Fig. 4B. Detail of the element support.

where:

- the section corner radius (r_c) is normalized with respect to the section width (b_w);
- the effective bond length (l_e) is defined as the length value beyond which there is no increase of the force transferred between concrete and FRP:

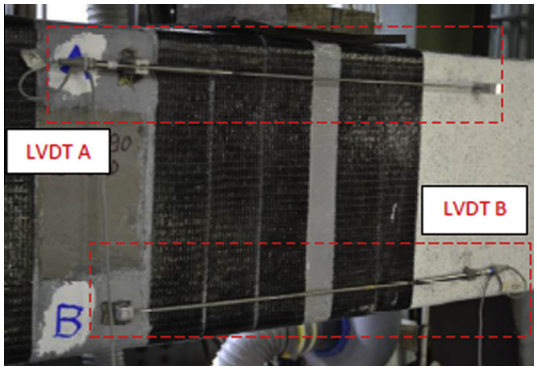

Fig. 5. Horizontal displacement transducers (LVDT A, B).

$$l_e = min\left\{\frac{1}{\gamma_{rd} f_{bd}}\sqrt{\frac{\pi^2 E_f t_f \Gamma_F}{2}}, 200\ \text{mm}\right\} \tag{2b}$$

where $f_{bd} = 2\Gamma_{Fd}/s_u$ (with $s_u = 0.25$ mm) and $\gamma_{rd} = 1.25$.

According to the guideline the value of fracture energy Γ_F is:

$$\Gamma_{Fd} = k_G\sqrt{\frac{2-\frac{b_f}{p_f}}{1+\frac{b_f}{p_f}}} \times \sqrt{f_{cm}\cdot f_{ctm}} \quad \text{with } \frac{b_f}{p_f} \geqslant 0.25 \tag{2c}$$

where

- f_{cm} and f_{ctm} are the mean value of the concrete cylindrical compressive strength and the concrete tensile strength respectively
- k_G is a coefficient equal to 0.037 (dimensionally in mm) for the CFRP strips adopted in the experimental tests.

- the ultimate design strength for debonding (f_{fdd}) is computed according to:

$$f_{fdd} = \frac{1}{\gamma_{fd}}\cdot\sqrt{\frac{2\cdot E_f\cdot\Gamma_{Fd}}{t_f}} \tag{2d}$$

where $\gamma_{fd} = 1.0$ was assumed.

According to the ACI code [12], the shear FRP resistance can be evaluated by adding the FRP contribution (V_f) to the concrete (V_c) and steel (V_s) (stirrups, ties or spirals) contributions (see Eq. (3)).

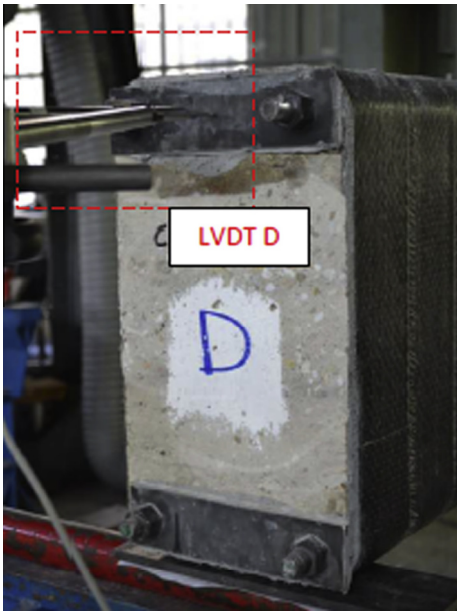

Fig. 6. Horizontal displacement transducers (LVDT C,D).

Fig. 7A. Element REF after collapse: crack path.

Fig. 7B. Element REF after collapse: concrete punching at the support.

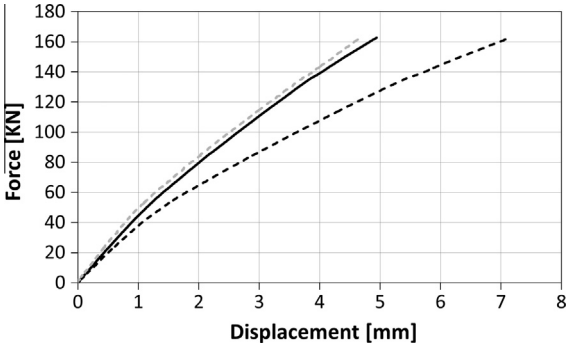

Fig. 8A. Force-displacement curves: LVDT 1 (continuous black line), LVDT 2 (dotted black line), LVDT 3 (dotted gray line).

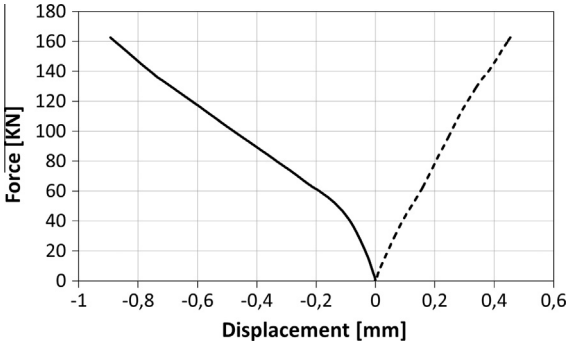

Fig. 8B. Force-displacement curves: LVDT A (dotted black line), LVDT B (continuous black line).

$$\phi V_n = \phi \cdot (V_c + V_S + \psi_f \cdot V_f) \tag{3}$$

where ϕ is a global strength reduction factor (to be assumed equal to 0.75, according to ACI) and ψ_f (equal to 0.95 for fully wrapped sections) is a reduction factor that takes into account the contact critical situation.

V_f can be evaluated by means of Eq. (4):

$$V_f = \cdot d \cdot E_f \cdot \varepsilon_f \cdot 2 \cdot t_f \cdot \frac{b_f}{p_f} \tag{4}$$

which assumes a concrete truss angle of 45° and an ultimate FRP strain $\varepsilon_f = 0.004 \leqslant 0.75\ \varepsilon_{fu}$. This is lower than the ultimate FRP axial strain (ε_{fu}) to take into account the loss of aggregate interlock in concrete.

3. The strengthening system

The confinement of RC columns is usually obtained through the application of FRP sheets wrapped directly on the concrete surface, using resins.

In the case of elements subjected to combined flexural and axial loads, a load carrying capacity increase can be achieved by means of a combined confinement: four rounded corners, L-shaped steel profiles are placed in the corners of the columns and are mutually connected by means of FRP strips. Construction stages are the following:

- concrete corners rounding;
- concrete surface preparation;
- steel profiles application;
- application of mortars in order to fill the space in between the steel profiles;
- FRP discrete wrapping application.

Fig. 9. Element CW90/30 after collapse: (A) Crack path, (B) Concrete detachment at the extrados and (C) Concrete detachment at the intrados.

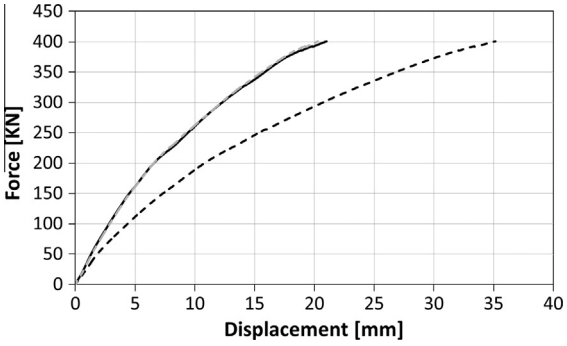

Fig. 10A. Force-displacement curves: LVDT 1 (continuous black line), LVDT 2 (dotted black line), LVDT 3 (dotted gray line).

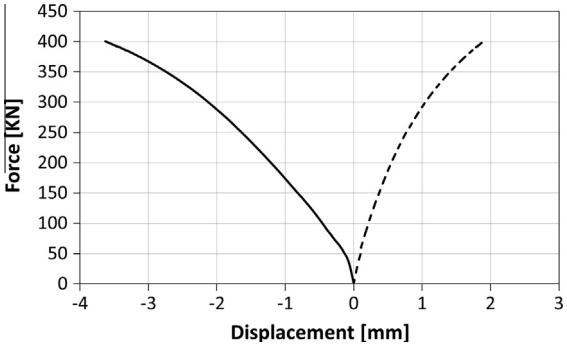

Fig. 10B. Force-displacement curves: LVDT A (dotted black line), LVDT B (continuous black line).

Fig. 11. Element CW90-8.6/30 after collapse: crack path.

The wrapping layouts adopted for the tested elements are reported in Fig. 2.

The previously described technology gives rise to both axial [11] and shear strength increases.

In order to better understand the behavior of reinforced concrete structural elements strengthened by means of the above technology an experimental campaign was carried out on 9 specimens. The first specimen is a reference element without external reinforcements, whereas the other eight differ from one another in:

- wrapping configuration (traditional wrapping without steel profiles or CFRP discrete wrapping and steel profiles, with or without filling mortar);
- FRP distribution in terms of wrapping spacing and number of layers.

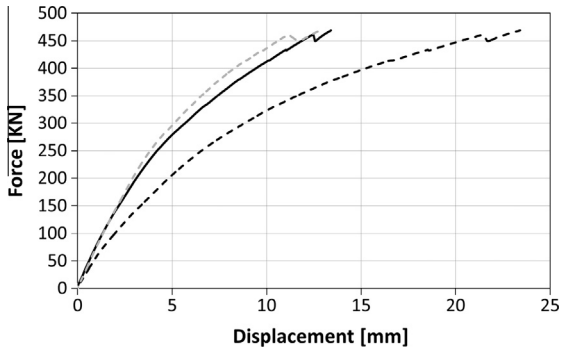

Fig. 12A. Force-displacement curves: LVDT 1 (continuous black line), LVDT 2 (dotted black line), LVDT 3 (dotted gray line).

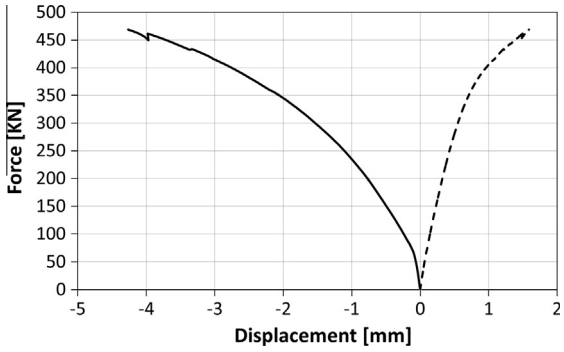

Fig. 12B. Force-displacement curves: LVDT A (dotted black line), LVDT B (continuous black line).

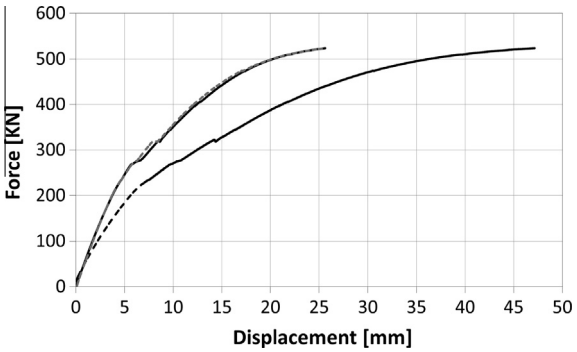

Fig. 14A. Force-displacement curves: LVDT 1 (continuous black line), LVDT 2 (dotted black line), LVDT 3 (dotted gray line).

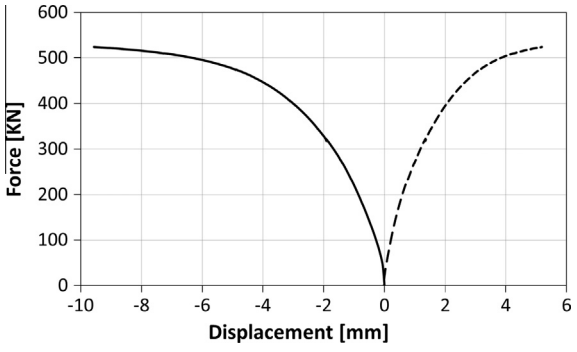

Fig. 14B. Force-displacement curves: LVDT A (dotted black line), LVDT B (continuous black line).

4. Specimen geometry

The nine specimens were designed in order to induce shear failure. To this purpose high strength steel longitudinal reinforcement was adopted. In order to clearly identify the FRP shear contribution, no steel stirrups were included in the concrete elements. Moreover, with the aim of emphasizing the FRP shear contribution, no axial force was applied during the tests, since it is well established that the axial force markedly increases the effect of aggregate interlock inside the shear cracks. The main objective was to reproduce the stress distribution in a vertical segment of an RC frame, that is characterized by a constant shear force and a linear bending moment. This was induced by imposing a vertical force at the midspan by restraining the element on two hinge supports with 3250 mm span length.

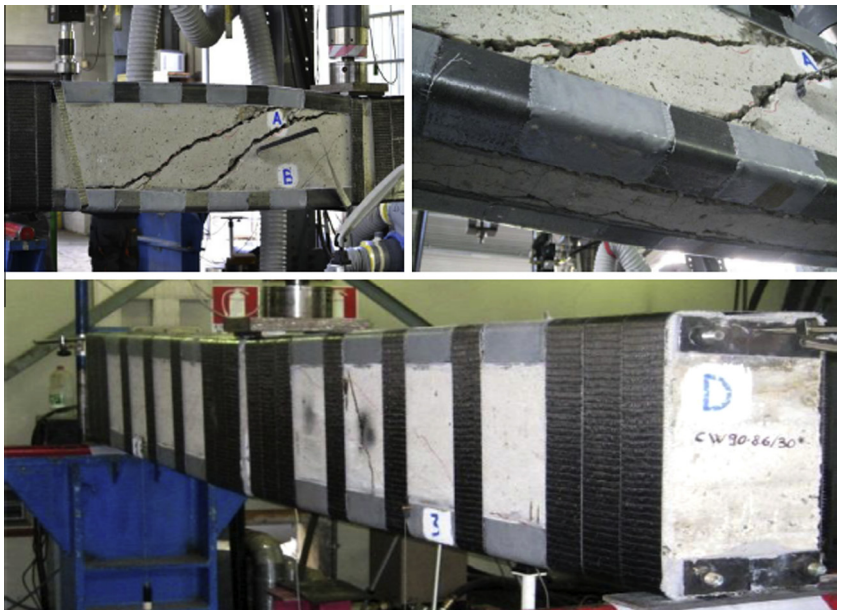

Fig. 13. Element CW90-8.6/30* after collapse: crack path.

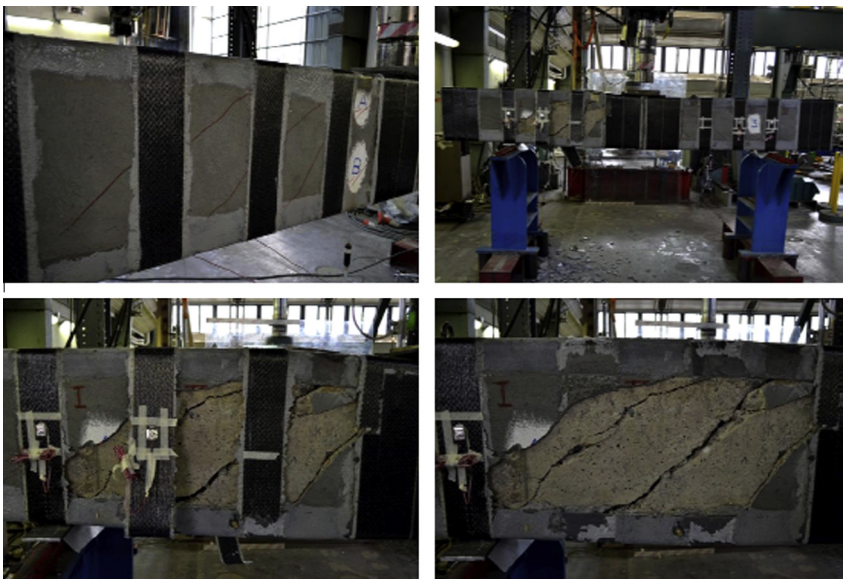

Fig. 15. Element CW90-8.6/30D after collapse: crack path.

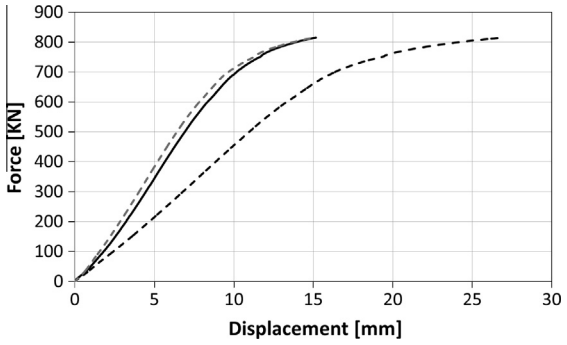

Fig. 16A. Force-displacement curves: LVDT 1 (continuous black line), LVDT 2 (dotted black line), LVDT 3 (dotted gray line).

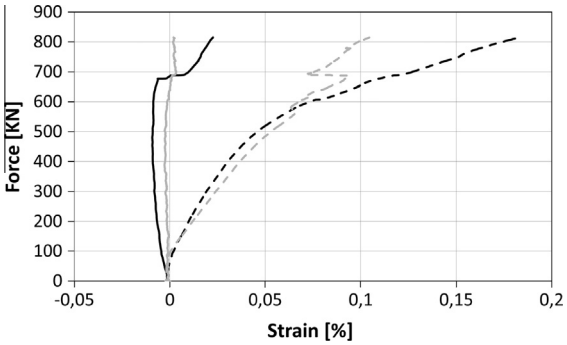

Fig. 16B. Force-strain curves: SG 1 (continuous black line), SG 2 (dotted black line), SG 3 (dotted gray line), SG 4 (continuous gray line).

All the specimens are characterized by the same geometry and steel reinforcement, namely:

- cross section 250 × 450 mm;
- length 3450 cm;
- longitudinal steel reinforcement constituted by 3 ϕ 20 mm bars placed at the top and 5 or 7 ϕ 20 mm bars placed at the bottom of the element.
- some steel stirrups (6 mm diameter bars and 50 mm spacing) were placed only at the supports and at the midspan of the elements (where the load is applied);
- three additional CFRP double layer wrappings were placed at the supports and six at midspan.

The reference specimen, named REF, had no shear FRP reinforcement while the others were characterized by different configurations of FRP strips (200 mm width) placed with different spacing. The geometries of the reinforcement in the nine specimens are reported in Table 1. Each specimen had an identifying name that characterizes the adopted strengthening strategy, given by combining the following abbreviations:

- CW90: Carbon Wrapping placed with a 90° angle;
- 8.6: L shaped steel profiles 6 mm thick and 80 mm wide;
- 12.8: L shaped steel profiles 8 mm thick and 120 mm wide;
- /N: wrapping spacing (/30 = 300 mm; /60 = 600 mm);
- D: double FRP layers;
- *: absence of thixotropic mortar filling;
- M+: extra longitudinal reinforcement designed in order to prevent flexural collapse.

The shear strengthening configurations adopted for the tested elements are summarized in Table 1 where the single layer of CFRP wrapping is represented in gray, while black color was used for double layers. In Fig. 3, some significant cross sections are visualized.

The mechanical properties of the materials were evaluated by means of specific tests. Six tests on cubic concrete specimens were performed and a mean cubic compressive strength (R_{cm}) of 22.67 MPa was obtained, which corresponds to a mean cylindrical compressive strength (f_{cm}) of 18.82 MPa. Note that the low value of the concrete strength matches the assumption that the tested elements simulate old RC structural elements. Furthermore, the following derived quantities were evaluated according to the Italian code NTC2008 [16]:

- Young Modulus E_{cm}:

$$E_{cm} = 22000 \cdot \left(\frac{f_{cm}}{10}\right)^{0.3} = 26595 \text{ MPa} \tag{5}$$

Fig. 17. Element M + CW90-8.6/30D after collapse.

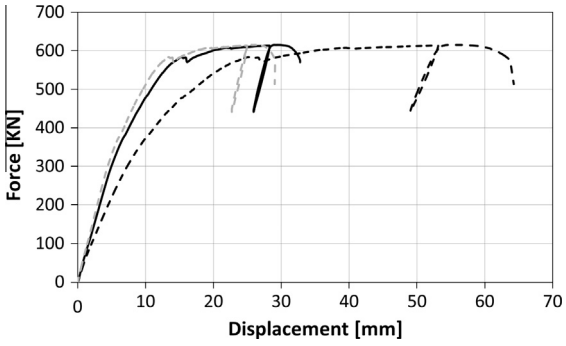

Fig. 18A. Force-displacement curves: LVDT 1 (continuous black line), LVDT 2 (dotted black line), LVDT 3 (dotted gray line).

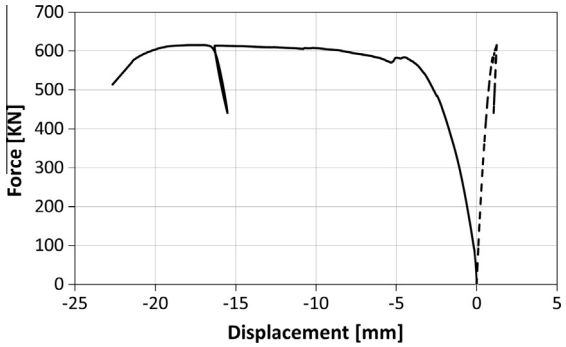

Fig. 18B. Force-displacement curves: LVDT A (dotted black line), LVDT B (continuous black line).

- mean tensile strength f_{ctm}:

$$f_{ctm} = 0.3 \cdot (f_{cm} - 8)^{(2/3)} = 1.467 \text{ MPa} \quad (6)$$

Two different types of steel were used for the reinforcement. Tensile tests were performed to determine steel properties (see Fig. 4) and the following mechanical characteristics were determined:

(1) 6 mm diameter stirrups: yielding stress and strength larger than 450 MPa and 540 MPa respectively, elastic modulus of 205 GPa and ultimate strain greater than 16.0%;

(2) Longitudinal reinforcement (threaded bars of the quality ASTM A193/B7): yielding stress and strength greater than 600 MPa and 850 MPa, respectively, elastic modulus of 188 GPa and ultimate strain greater than 3%, tested in laboratory according to UNI EN ISO 15630-1.

Unidirectional carbon fiber wraps (mass per unit area equal to 400 g/m^2) with nominal thickness of 0.225 mm were used as CFRP reinforcement. Tensile strength and Young modulus of the CFRP sheets were evaluated by means of standard "coupon test", performed on three specimens 20 mm wide and 300 mm long. The mean values of the Young modulus E_{fib} and of the tensile strength f_{fib} (both estimated with respect to the area of fibers only, as indicated in the Italian guidelines [13]) were 392.7 GPa and 2824 MPa, respectively.

5. Experimental set-up

The specimens were tested by adopting a three point bending configuration (see Fig. 4A), by means of an hydraulic jack (1000 kN maximum load) with displacement control at 1 mm/min velocity. The load was applied at midspan by means of a steel plate located between the jack and the RC element. A rubber layer was placed under the distribution plate in order to ensure flatness of the contact surface and a steel plate with a Teflon layer were placed over the two cylindrical supports in order to reduce friction (Fig. 4B).

The displacements during the test were measured by means of:

- three core free vertical transducers (LVDT 1,2,3) to measure the vertical displacement of three points, namely at midspan and at 1/4 of the total length, from the nearest support (see Fig. 4A);
- two horizontal displacement transducers (LVDT A, B) positioned at midspan to measure the axial shortening of the top fiber and the elongation of the bottom fiber (see Fig. 5);
- two horizontal displacement transducers (LVDT C, D) located at the two extreme sections of the element to measure possible rotations of the section (see Fig. 6);
- Strain Gauges (I, II, III and IV), positioned on the CFRP strips to measure their deformation during the experiments. This last instrumentation was used only for the tests CW90-8.6/30D and CW90-8.6/30D*.

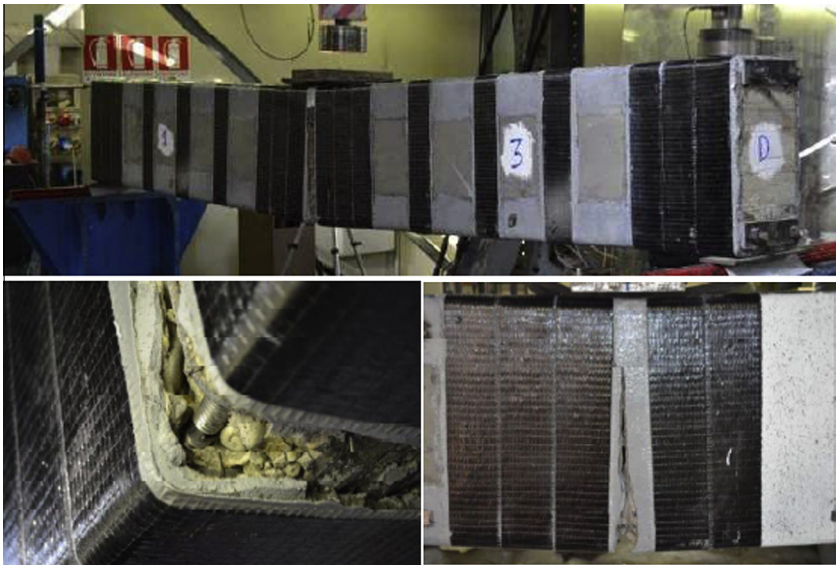

Fig. 19. Element M + CW90-12.8/30D after collapse.

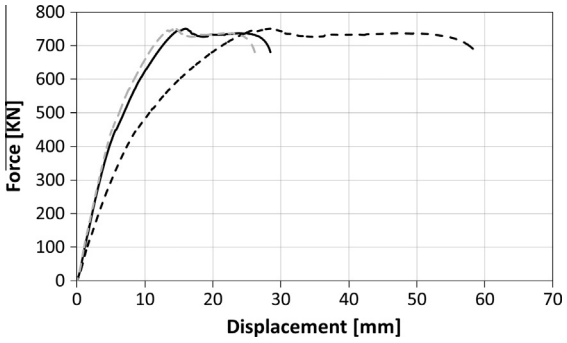

Fig. 20A. Force-displacement curves: LVDT 1 (continuous black line), LVDT 2 (dotted black line), LVDT 3 (dotted gray line).

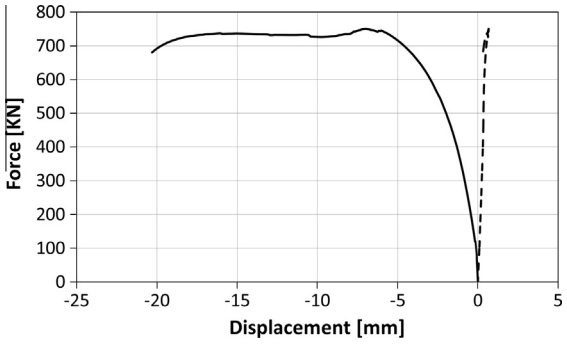

Fig. 20B. Force-displacement curves: LVDT A (dotted black line), LVDT B (continuous black line.

6. Tests results

The nine tests performed are described in the following.

6.1. REF

Failure occurred at a total load value of 162.74 kN (see Fig. 8), with a vertical displacement at midspan of 7.16 mm. A typical brittle shear failure was observed due to the absence of any transversal reinforcement: a diagonal crack (see Fig. 7A) started near midspan, propagated along ¼ of the total length, and finally extended along the intrados of the element to the support. The test was then extended beyond the peak load because of the activation of an arch resisting mechanism that vanished due to the slipping of the three (not anchored) lower longitudinal bars (Fig. 7B).

6.2. CW90/30

The global failure can be attributed to the breaking of one CFRP strip, followed by the rupture of the others strips on the same side of the element. Due to this phenomenon, failure in concrete is characterized by diagonal cracks with a truss angle value θ of $\cong 45^{\circ}$ (Fig. 9A). The concrete cover detachment can be observed, at the intrados and extrados of the element (Fig. 9B and C). Failure occurred at a load value of 400.59 kN, with a vertical displacement at midspan of 35.14 mm (see Fig. 10A).

6.3. CW90-8.6/30

The crack path shows the classical strut and tie mechanism, characterized by a truss angle value θ of $\cong 36^{\circ}$ (Fig. 11). Failure occurred at 468.83 kN (see Fig. 12), with a vertical displacement at midspan of 23.41 mm. The shear failure of the element was induced by the rupture of one strip of CFRP (single layer).

If compared with the test on specimen CW90/30 (that does not hold the steel profiles) a shear strength increment of 35 kN and a reduced truss angle value (θ) can be observed. This small increment in the shear strength is therefore explained in view of the different strut angle rather than for the contribution of the steel profiles.

6.4. CW90-8.6/30*

A brittle failure was caused by the rupture of a strip of CFRP (followed by the rupture of the others), with consequent deep diagonal cracks in concrete. Cracks across the element outlined a strut mechanism with a truss angle value θ of $\cong 30^{\circ}$ (Fig. 13). Failure occurred at a load value of 523.67 kN (Fig. 14), with a vertical displacement at midspan of 53.73 mm. Comparing this test with the previous one (i.e. CW90-8.6/30), which differs only for the presence of thixotropic mortar between FRP and the concrete

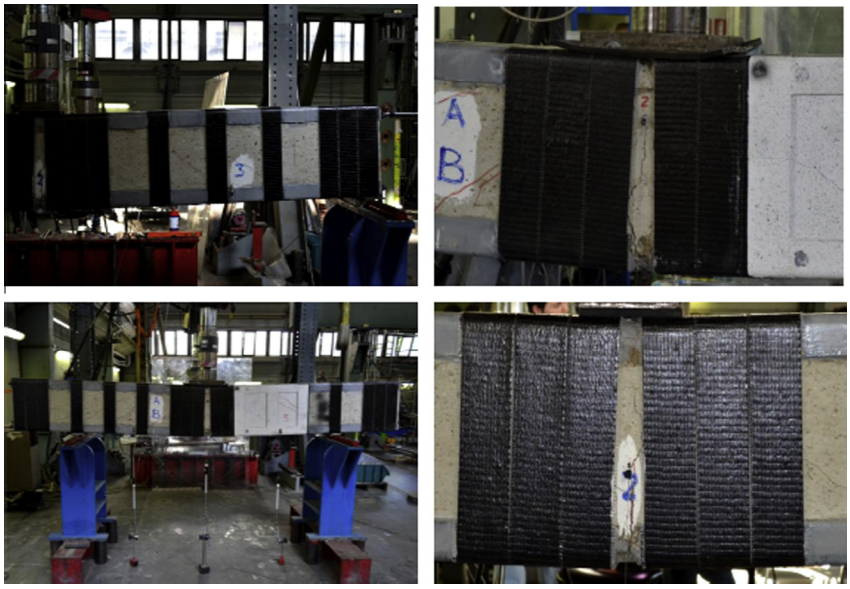

Fig. 21. Element CW90-8.6/30D° after collapse.

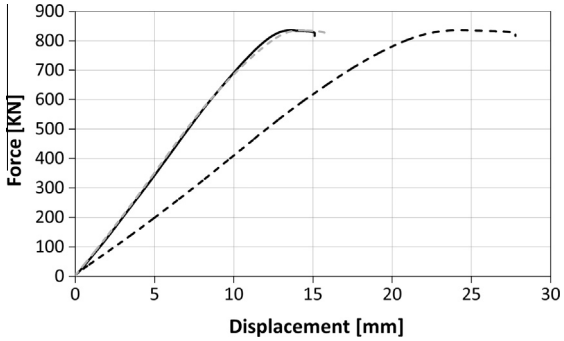

Fig. 22A. Force-displacement curves: LVDT 1 (continuous black line), LVDT 2 (dotted black line), LVDT 3 (dotted gray line).

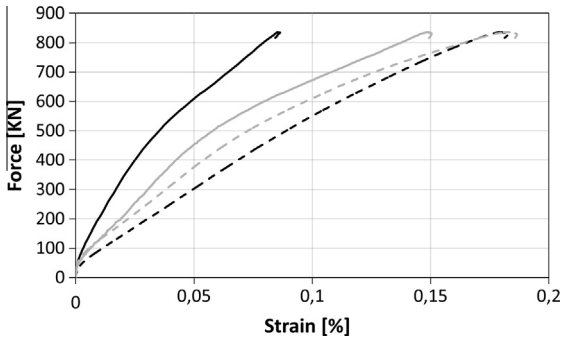

Fig. 22B. Force-strain curves: SG I (continuous black line), SG 2 (dotted black line), SG 3 (dotted gray line), SG 4 (continuous gray line).

surface, a load increase of 55 kN can be observed. This phenomenon can be attributed to the gap between the FRP and the concrete surface that induces smaller transversal strain into the CFRP strip. During the test, the vertical displacement transducer placed at midspan (named LVDT 2) malfunctioned because of a diagonal crack that opened on the contact surface; therefore the force-displacement curve of LVDT 2 visualized in Fig. 14 at high load levels comes from the output of the jack instrumentation.

6.5. CW90-8.6/30D

The experiment was carried out in three phases:

(1) the first test was interrupted due to a yielding of the longitudinal reinforcement. The maximum load achieved was 455.33 kN, with a vertical displacement at midspan of 26.37 mm. Although the element was not interested by a shear failure, the crack path outlined a strut mechanism in concrete;
(2) the same specimen previously tested was reloaded with a new strip of CFRP added at midspan. The element did not fail due to a ductile mechanism activated during the test (yield strength of the bars). Also this test was interrupted, after reaching a maximum load of 455.14 kN and a vertical displacement at midspan of 22.21 mm;
(3) the damaged element was tested again after reducing the span length to 2.35 m. Four strain gauges were placed on the CFRP strips in order to measure its strain during the test. In this last case shear failure occurred because of the rupture of the CFRP wrappings at a peak load of 815.21 kN, with a vertical displacement at midspan of 26.99 mm. The truss angle value θ was $\cong 45^{\circ}$ (Fig. 15). The data acquired during the test are drawn in Fig. 16.

6.6. M+CW90-8.6/30D

The maximum measured load was 615.31 kN, with a vertical displacement at midspan of 68.51 mm. In the final part of the experiment, an unloading-reloading cycle of 150 kN, was carried out. Failure occurred because of breaking of the longitudinal rebars and debonding of the additional bars placed in the middle of the element (Fig. 17). The experimental results are shown in Fig. 18.

6.7. M+CW90-12.8/30D

This test was carried out up to a load of 750.8 with a vertical displacement of 58.69 mm. At such ultimate load the activation of a flexural mechanism was observed with the pull-out of the additional steel bars placed in the middle of the element (see Fig. 19).

The data acquired during the test are visualized in Fig. 20.

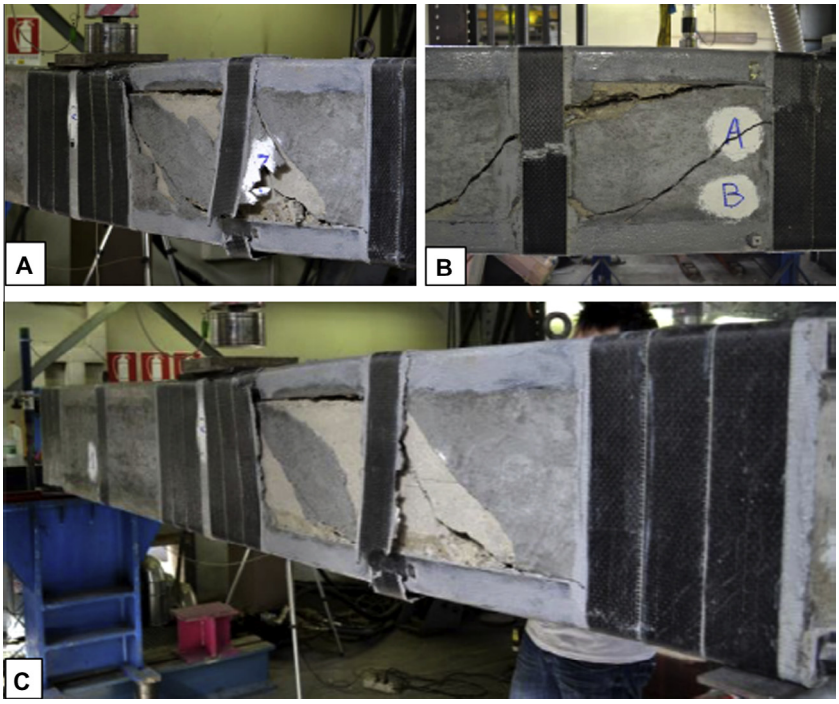

Fig. 23. Element CW 90-8.6/60 after collapse: crack path.

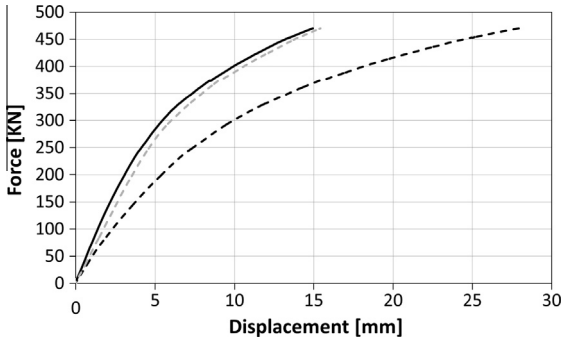

Fig. 24A. Force-displacement curves: LVDT 1 (continuous black line), LVDT 2 (dotted black line), LVDT 3 (dotted gray line).

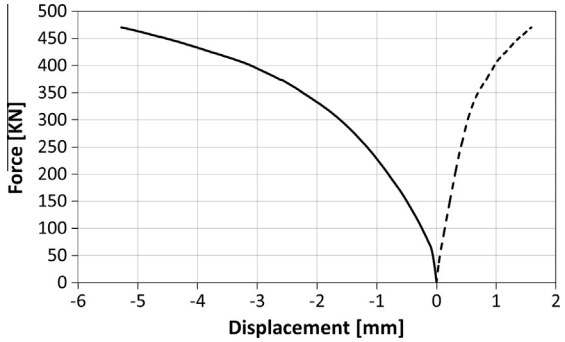

Fig. 24B. Force-displacement curves: LVDT A (dotted black line), LVDT B (continuous black line).

*6.8. CW90-8.6/30D**

Similarly to specimen CW90-8.6/30D, this test was performed in three stages:

(1) The specimen was firstly loaded up to 540.5 kN, when the vertical displacement measured at midspan was 61.30 mm. During the test the vertical displacement transducer at midspan did not work correctly, so the force-displacement curve was obtained from the jack instrumentation;
(2) the same element, previously tested, was reloaded without any instrumentation. The shear failure was not reached because of yielding of the longitudinal bars;
(3) a new test configuration was adopted on the same damaged element, by reducing the span length to 2.35 m. Four strain gauges were placed on the CFRP strips in order to measure its strain during the test. In this last case flexural failure occurred because of breaking of the longitudinal reinforcement, at a load value of 835.98 kN, corresponding to a vertical displacement at midspan of 27.8 mm (Fig. 21). The data acquired during the test are reported in Fig. 22.

6.9. CW90-8.6/60

Failure occurred at a load value of 470.30 kN, with a vertical displacement at midspan of 27.93 mm. The shear failure of the element was induced by breaking of one strip of CFRP (single layer), with consequent deep diagonal cracks growth along the element. The crack path shows the classical strut and tie mechanism developed in concrete, with a truss angle value θ of $\cong 33^{\circ}$. This phenomenon is underlined by the steel corner deformation (on the upper side) following the explosive collapse of the CFRP strips (Fig. 23). The data acquired during the test are visualized in Fig. 24.

7. Discussion of the results

A summary of the experimental results in terms of: maximum shear and bending moment, vertical displacement at midspan and type of failure, is shown in Table 2. A comparison between all load-displacement curves obtained from the tests is shown in Fig. 25.

First of all the high resistance of each specimen with respect to the reference one can be pointed out: the minimum strength is 2.45 times the reference value. Furthermore it has to be underlined the improved performance of the elements strengthened with steel profiles, especially when the CFRP strips are not attached to the concrete surface. Comparing the peak strengths of the three specimens CW90/30, CW90-8.6/30and CW90-8.6/30* it is possible to observe a gradual increase that, starting from the value of 440.6 kN (CW90/30 specimen without steel profiles) becomes 468.8 kN for the specimen CW90-8.6/30 with steel profiles and filling mortar-, and 523.7 kN for the specimen CW90-8.6/30* with steel profiles and without mortar, i.e. CFRP strips detached from concrete surface. The strength increase with respect to the unreinforced element, is respectively equal to 145%, 188% and 222%. This trend depends on both a better performance of the FRP strips, whose load carrying capacity is less affected by the cracks evolution and by stress localizations and on the decrease of the strut angle θ at the ultimate limit state. This outcome points out the importance of including a reduction factor related to the debonding across the cracks in the evaluation of the FRP strip strength.

In view of the experimental results described above, it can be also stated that:

(1) With reference to specimens CW90-8.6/30 and CW90-8.6/60 we observe that the wrapping spacing increase (from 300 to 600 mm) did not reduce the element strength. This can be explained in view of the fact that, when three strips are present, the truss mechanism developed involves primarily the CFRP strip positioned in the middle, whereas the peripherals are almost unstressed, see Figs. 9–23.

(2) The increase of the CFRP strip thickness (i.e. 2 layers are adopted instead of one) gave rise to a significant strength increase. This is evident comparing for instance specimens CW90-8.6/30D and CW90-8.6/30. This outcome is obvious since collapse occurs because of a CFRP strip breaking. Nevertheless, the span length reduction adopted in order to avoid flexural collapse might have affected somehow the test result for specimen CW90-8.6/30D.

8. Code predictions

In Table 3, the experimental results for the elements that collapsed because of shear failure are compared with the results obtainable by means of the Italian guidelines [13] and American code [12]. In these computations, in order to use predictive equations, both the partial safety factor γ_{Rd} (see Eq. (1)) and the reduction factor ϕ (see Eq. (3)) were assumed equal to 1.0, and in Eq. (2d) the characteristic compressive strength f_{ck} was replaced by the mean compressive strength f_{cm}.

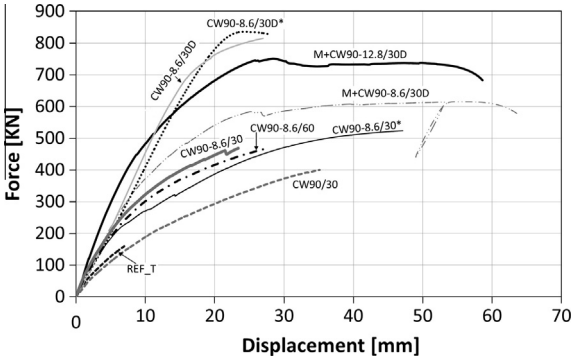

Fig. 25. Force-displacement curves for all tested elements.

Regarding the concrete contribution V_c in Eq. (3) (lack of stirrups means $V_s = 0$) it has to be specified that the ACI FRP code [12] has to be applied together with the ACI concrete code [17], that is:

$$V_c = 2\lambda \cdot \sqrt{f_c'} \cdot b_w \cdot d = 71.9 \text{ kN} \tag{7}$$

where:

- f_c' is the compressive strength of concrete in [psi] (in Table 3 the mean compressive strength f_{cm} was adopted);
- b_w and d are width and depth of effective cross section, respectively.

Table 3 shows that predictions made by using the ACI code underestimates the shear load carrying capacity of a traditional RC element. This outcome is frequent (see for instance [18]), but nevertheless is similar to the forecast made in both European and American codes when dealing with a traditional reinforced concrete element equipped with steel stirrups.

It is well known that the classical shear analysis of Ritter and Mörsch ([8–10]) explains the shear strength in the cracked state by a truss analogy. The bottom chord of the truss is formed by the longitudinal reinforcement, the top chord by the concrete in the compression zone, the tension web members by the stirrups, and the compression web members by concrete struts in the web of the element. However, laboratory tests indicated that the stresses developed in the web reinforcement (the stirrups) were less than those calculated by means of this assumption [19]. This is the reason why in previous editions of the Italian Technical Standards for Construction [16] shear strength was computed as the sum of a term related to the web reinforcement (V_{wd}) and a term related to the shear strength of the uncracked concrete in the compression chord (V_{cd}).

Table 2
Summary of all the experimental results.

Test	Experimental tests				
	F_{max} (kN)	V_{max} (kN)	M_{max} (kNm)	u_{max} (mm)	Failure mode
REF	162.74	81.37	132.23	7.16	Shear
CW90/30	400.59	200.30	325.48	53.73	Shear
CW90-8.6/30	468.83	234.42	380.92	36.43	Shear
CW90-8.6/30*	523.67	261.84	425.48	26.37	Shear
CW90-8.6/30D A	455.33	227.67	369.96	27.90	Bending
CW90-8.6/30D B	455.14	227.57	369.80	68.51	Bending
CW90-8.6/30D C	815.21	407.61	662.36	58.69	Shear
M + CW90-8.6/30D	615.31	307.66	499.94	27.93	Bending
M + CW90-12.8/30D	750.80	375.40	610.03	23.41	Bending
CW90-8.6/30D* A	540.50	270.25	439.16	22.21	Bending
CW90-8.6/30D* B	541.60	270.80	440.05	26.99	Bending
CW90-8.6/30D* C	835.98	417.99	679.23	35.14	Bending
CW90-8.6/60	470.30	235.15	382.12	61.30	Shear

Table 3
Comparison between experimental results and codes previsions.

		Experiment	CNR DT200/2012				ACI 440.2R-02	
		V_{exp} (kN)	θ (°)	$V_{rd,f}$ (kN)	$V_{rd,1}$ (kN)	$V_{rd,2}$ (kN)	V_f (kN)	V_n (kN)
1	REFT	81.37	\	\	91.2	\	\	\
2	CW90/30	200.30	45	40.3	131.5	152.5	94.2	166.2
3	CW90-8.6/30	234.42	36	55.4	146.6	209.9	94.2	166.2
4	CW90-8.6/30*	261.84	30	69.8	161.0	264.1	94.2	166.2
5	CW90-8.6/30D	407.61	45	61.8	153.0	305.0	188.5	260.4
6	CW90-8.6/60	235.15	33	48.4	139.6	234.8	94.2	166.2

Currently the Italian Technical Standards for Construction [16] and the CNR guidelines [13] require, in accordance with the European Code [15], that the shear force is fully carried by the web members (i.e. $V_{Rd,s} = V_{wd}$). As a consequence the CFRP strengthened element load bearing capacity, in case of fully wrapped configuration, is drastically underestimated (see column $V_{Rd,f}$ in Table 3). To overcome this inconsistency two proposals are here outlined:

1. No updating is needed in the definition of the FRP shear resistance (i.e. Eq. (1b) remains unchanged), but the shear strength of the element should be computed by taking into account the term V_{cd} (i.e. $V_{Rd,s} = V_{wd} + V_{cd}$), according to the previous edition of the CNR guidelines [20]. This solution gives rise to the outcomes written in column $V_{Rd,1}$ of Table 3.
2. In the case of completely wrapped members collapse occurs because of breaking of the carbon strips, especially when these wrappings are detached from concrete, and therefore bond length (and fracture energy too) become meaningless. In view of this circumstance in Eq. (1b) the material strength f_{fd} (equal to 2824 MPa according to experimental tensile tests) should be used instead of f_{fed} (solution that gives rise to the outcomes written in column $V_{Rd,2}$ of Table 3).

9. Conclusions

The validation of a new strengthening technology that combines L shaped steel profiles and discrete CFRP wrapped sheets has been performed by means of the outputs of nine experimental tests. These test show that the longitudinal steel profiles placed along the section corners indirectly increase the shear capacity of an RC element since they allow to create a gap between the concrete surface and the FRP: this gap avoids stress concentration in the FRP strips where they cross the concrete cracks.

The shear load carrying capacity of the strengthened elements turned out to be more than doubled (with respect to that of the non-strengthened one). Nevertheless, it has to be stated that, in order to show the enhancement due to CFRP external reinforcement, the test configurations adopted are the most favorable: no stirrup was placed inside the concrete specimens in the critical zones and the axial force (usually very important in a column) was not applied (so as to reduce the aggregate interlock in the cracks).

When adopting this technology (FRP is detached from the concrete surface) an external jacketing is needed to protect the CFRP wrapping from accidental impacts and acts of vandalism. Nevertheless, a jacketing (that in this case could be for instance made of timber panels) is usually needed for fire protection, independently of the technology adopted for the FRP wrapping.

The results of the experimental tests have been then compared with the predictive equations suggested by the American and Italian code. The peculiarities of the unconventional strengthening method proposed are not taken into account by the ACI code, whose prediction is nevertheless on the safe side and the error gathered is of the same extent than the one that can be made when dealing with a traditional reinforced concrete element equipped with steel stirrups. On the contrary the chapter of the Italian code that deals with the case of shear strength of completely wrapped members (i.e. columns) needs revision.

Acknowledgements

This study is part of a research project financed by Interbau S.r.l., Milan, that prepared the reinforced concrete specimens and applied the CFRP layers too. The authors express their thanks to Interbau S.r.l. for the financial and technical support. Part of the analyses were developed within the activities of Rete dei Laboratori Universitari di Ingegneria Sismica – ReLUIS for the research program funded by the Dipartimento di Protezione Civile – Progetto Esecutivo 2010–2013.

References

[1] Taljsten B. Strengthening of concrete structures for shear with bonded CFRP fabrics. In: Meier U, Betti R, editors. Recent advances in bridge engineering. Switzerland: EMPA; 1997. p. 67–74.
[2] Triantafillou TC. Shear strengthening of reinforced concrete beams using epoxy-bonded FRP composites. ACI Struct J 1998;95(2):107–15.
[3] Chen JF, Teng JG. Shear capacity of fiber-reinforced polymer-strengthened reinforced concrete beams: fiber reinforced polymer rupture. ASCE J Struct Eng 2003;129(5):615–25.
[4] Chen JF, Teng JG. Shear capacity of FRP-strengthened RC beams: FRP debonding. Constr Build Mater 2003(17):27–41.
[5] Monti G, Liotta MA. Tests and design equations for FRP-strengthening in shear. Constr Build Mater 2007;21(4):799–809.
[6] Teng JG, Chen GM, Chen JF, Rosenboom OA, Lam L. Behavior of RC Beams Shear Strengthened with Bonded or Unbonded FRP Wraps. J Compos Constr 2009;13:394–404.
[7] Bocciarelli M, di Feo C, Nisticò N, Pisani MA, Poggi C. Failure of RC beams strengthened in bending with unconventionally arranged CFRP laminates. Compos B 2013;54:246–54.
[8] Ritter W. Die Bauweise Hennebique. Schweizerische Bauzeitung (Zurich) 1899;33(7):59–61.
[9] Mörsch E. Versuche uber Schubspannungen in Betoneisentragern. Beton und Eisen (Berlin) 1903;2(4):269–74.
[10] Mörsch E. Concrete-steel construction, E.P. Goodrich, translation of "Der Eisenbetonbau", McGraw-Hill, New York, 1909.
[11] Monti G, Nisticò N. Square and rectangular concrete columns confined by C-FRP: experimental and numerical investigation. Mech Compos Mater 2008;44(3):289–308.
[12] ACI 440.2R-02 – Guide for design and construction of externally bonded frp systems for strengthening concrete structures. American Concrete Institute, 2002.
[13] National Research Council. CNR-DT200 R1/2012 – guide for the design and construction of externally bonded FRP systems for strengthening existing structures. Rome: CNR; 2012.
[14] Priestley MJN, Verma R, Xiao Y. Seismic shear strength of reinforced concrete columns. ASCE J Struct Eng 1994;120(8):2310–29.
[15] European Committee for Standardization. Eurocode 2: Design of Concrete Structures – Part 1-1. General rules and rules for buildings. Brussels: CEN, 2004.
[16] Consiglio Superiore dei Lavori Pubblici. Norme Tecniche per le Costruzioni. DM 14/1/2008, Rome: Gazzetta Ufficiale n. 29 del 4/2/2008 – Suppl. Ordinario n. 30.
[17] ACI 318-08 – Building Code Requirements for Reinforced. American Concrete Institute, 2008.
[18] Russo G, Somma G, Angeli P, Guerrini G. Shear strength analysis for normal and high-performance concrete beams. In: Proceedings of 6th International Symposium on "Utilization of High Stregth/High Performance Concrete". Lipsia, Germany, 2002. p. 553–67.
[19] Richart FE. An Investigation of Web Stresses in Reinforced Concrete Beams. Bulletin No. 166, University of Illinois Engineering Experiment Station, Urbana, June 1927. p. 103.
[20] National Research Council, CNR-DT200/2004 – Guide for the Design and Construction of Externally Bonded FRP Systems for Strengthening Existing Structures. Rome: CNR, 2004.